# COMPUTATIONAL MODELING OF THERMAL CONDUCTIVITY OF RANDOM PARTICULATE COMPOSITES WITH CONTACT RESISTANCE

Dongfang Zhao, Yizhan Zhang, & Yun-Bo Yi\*

Department of Mechanical and Materials Engineering, University of Denver, Denver, Colorado 80208, USA

\*Address all correspondence to: Yun-Bo Yi, Department of Mechanical and Materials Engineering, University of Denver, Denver, CO, USA 80208, E-mail: yyi2@du.edu

Original Manuscript Submitted: 5/3/2021; Final Draft Received: 7/26/2021

The effective conductivity of a heterogeneous particulate material system is computationally investigated using the Monte Carlo scheme and the finite element method. The material is modeled as randomly dispersed, deformable ellipsoids considering interfacial contact including both Coulomb friction and contact resistance. A dynamic deployment algorithm for particle generation is implemented, followed by a steady-state heat conduction analysis with a constant temperature gradient across the boundaries, using the implicit numerical scheme. The simulations are performed to establish a quantitative relationship between the dimensionless conductivity and the various parameters including (1) volume fraction, (2) particle aspect ratio, (3) material stiffness, (4) coefficient of friction, and (5) thermal contact resistance. The computational results have revealed that the prolate particles produce the highest effective conductivity over the oblate or tri-axial ones, that the conductivity decreases with the particle aspect ratio, and that the contact resistance changes the effective conductivity based on a monotonic, yet nonlinear function.

**KEY WORDS:** thermal conductivity, contact resistance, particulate composite, friction

#### 1. INTRODUCTION

Heterogeneous particulate composites play an important role in modern industry. For example, friction materials are widely used in aircraft and aerospace, automobiles, railroad construction, and heavy machinery manufacturing (Solomon and Berhan, 2007). Depending on the application, friction material formulations consist of various particulate ingredients, both metallic and nonmetallic (Lu, 2006; Sriwiboon et al., 2018). Existing laws facilitate the removal of heavy metals in vehicle brake friction materials to reduce environmental exposure of these materials in waterways. Graphite (Aranganathan and Bijwe, 2016; Panda et al., 2016), carbon (Ye et al., 2016; Singaravelu et al., 2019), and ceramic (Kaźmierczak-Baiata and Mazur, 2018) are potential replacements for metals; however, the implementation of these new materials may introduce operational safety issues. For example, thermal conductivity is associated with the capacity of heat dissipation to prevent overheating (Li and Yan, 2017). It is unclear how the new materials (e.g., graphitic powders or ceramic compounds in place of metals) will alter tribological properties that can affect thermal stability (Zhao et al., 2015). In addition, during the manufacturing of friction linings or other particulate materials such as metal powders in laser powder bed fusion additive manufacturing (King et al., 2015; Volpp, 2019; Mussatto et al., 2021), enhanced thermal or mechanical properties result from pressing materials into higher volume fraction layers. It is essential to have a predictive tool to study the effect of various factors including material composition, microstructure, morphology, and manufacturing processes.

Multiscale modeling of heterogeneous carbon and graphite-related composites has been an active research area for many years. Approximations using the effective medium theories (EMTs) are widely available in the literature (Torquato, 2002), with examples including linear rules of mixing (Wei et al., 2004), Maxwell approximation

(Maxwell, 1873), self-consistent approximation (Gubernatis and Krumhansl, 1975), differential effective medium theory (Mclaughlin, 1977), and other theories applicable at low volume fractions (Mondescu and Muthukumar, 1999). It is also known that many of the material properties have a strong connection to the percolation problem (Sykes and Essam, 1963). A shortcoming of EMTs is the existence of numerical uncertainties (Garboczi and Berryman, 2001). In comparison, the *Monte Carlo method* is more efficient, especially for fillers of large aspect ratios (Zhang and Yi, 2008). Researchers have reported simulation results for spheres (Pike and Seager, 1974), ellipses (Qiu and Yi, 2018), ellipsoids (Yi et al., 2004), thin disks (Yi and Tawerghi, 2009; Qiu et al., 2015), and fibers (Cheng and Sastry, 1999). The *homogenization method* (Song and Youn, 2006; Fish and Fan, 2008) has also been a widely utilized tool, along with finite element analysis based on digital images (Cai et al., 2005; Chen et al., 2008). However, very few results were reported on the interfacial effects in the settings of contact mechanics, especially for nonspherical inclusions.

In this study we correlate the thermal conductivity of particulate composites to compression and packing, by incorporating the effects of friction and deformability of materials, using the finite element method. When particles are in physical contact, the thermal gradient across the interface can be appreciable and characterized by contact resistance (Yi, 2008). A study of contact resistance requires modeling of both thermal conduction and contact mechanics, which could be complicated due to the nonlinear relationship between the contact area and pressure (Kansal et al., 2002). In contrast, the nonlinearity in EMTs is primarily a result of solving the Laplace equation in multiphase media without considering contact mechanics. These models deal with two or three-phase composite systems, in which both the inclusions and matrix are conductive and the particles do not touch each other (Torquato and Rintoul, 1995). Also, the inclusions were assumed to be completely bounded by the matrix and the contact area was the entire surface of an inclusion (Wei and Poon, 2006). For dispersions of particles in a polymer matrix, however, the contact area is variable and generally smaller than the entire surface area of a particle (Wang et al., 2004). The coupling between mechanical deformation and thermal conductivity thus entails an iterative modeling technique incorporating dynamic deployment algorithm, interparticle contact, and thermal analysis with the consideration of contact resistance.

## 2. METHODS

Briefly, the simulation consists of three main steps: (1) particle generation and deployment, which is a dynamic process involving particle movement and rotation. Its algorithm is written in C programming language; (2) finite element analysis of particle compression using the commercial code ABAQUS/EXPLICIT. During the compression, the originally separate particles may come into contact under the pressure, therefore it is also an intrinsic, dynamic process; (3) finite element analysis of heat conduction. This is a static problem in which the particles cannot move and a steady-state heat conduction analysis is performed.

# 2.1 Particle Generation and Deployment Algorithm

We consider a system of randomly dispersed, impermeable, and equalized ellipsoidal inclusions distributed in a unit cell. The particles were generated with the incorporation of a series of dynamic collision algorithms. The particles were assumed to be tri-axial and the collisions were regarded as fully elastic so that no energy was lost during the process. The generation procedure of random particulate system not only required the center-point location to be dispersed randomly but also assumed the Euler angles of the axes to obey the prescribed density functions of probability. To avoid overlaps, the dynamic algorithms were deployed in which random parameters such as initial positions of the center-points of each inclusion and random velocities that allowed rigid body collision of particle—particle and particle—wall were assigned (Yi et al., 2006; Tawerghi and Yi, 2009). In the previous works, the so-called maximal packing fractions in a random particulate system were investigated by the deployment of growth algorithms. In the current study, we neglected the successive growth rate of the actual diameter since our intents were not concentrated on arranging particles to achieve maximum packing fractions, but we kept the technique of expanding the actual diameters with a size factor and performed collision processing with the expanded outer particles to guarantee that the actual particles were separated (Qiu and Yi, 2018).

The initial randomly generated particles were distributed in a unit cell. For spherical inclusions, the criterion for overlap detection is straightforward. However, it is more intensive to derive the contact or overlap criterion for

ellipsoidal inclusions, whose locations and geometries would be defined by not only the center-point location but also the orientation angles. The prior algorithm was adopted in the current study for overlap detection between two ellipsoids, in which each inclusion was given an initial velocity and rigid body collisions were allowed as mentioned previously. This algorithm was developed using C language and was run over thousands of iterations until there were no overlaps detected among the inclusions. The process usually ran 4000–5000 iterations, with a time step size set to 0.001. Also, the particle number and size were predetermined to ensure a constant initial volume fraction. The repulsive force couplings between the contacting particles were used to rectify the initial overlaps over particle—particle and particle—wall. Figure 1 shows computer generated, impermeable particulate systems.

# 2.2 Mechanical Modeling

In the second step, finite element meshing was performed on each generated ellipsoid from the first step. We assumed the system inclusions as shell particles in such a way that the conductive contents lay exclusively on the surfaces of particles. While volumetric conductivity is important in some applications, we focus our attention on conduction taking place on the particle surfaces only, due to the following reasons: (1) particle compression is in general a multibody dynamics problem that is very time consuming for finite element analysis. Using volumetric elements would involve an order of magnitude more degrees of freedom and therefore increase the computational effort considerably; (2) we encountered some numerical convergence difficulties with tetrahedral elements. The solution was found more stable using shell elements, possibly because the mechanical structure consisting of shell elements has a lower overall mechanical rigidity than that of volumetric elements.

The mesh generation of particles is a fundamental step in finite element analysis. In this study, we created a shell mesh with triangular elements on the surface of each inclusion using the built-in automatic mesh generation algorithms inside the commercial code COMSOL<sup>©</sup>. To avoid the possibility of inhomogeneous mesh density, which is curvature dependent, the parameters such as the curvature cutoff threshold and maximum element size were incorporated to prevent the occurrence of numerical inaccuracy that was caused by the local singularities. The triangular finite element meshing was first generated on a single particle, and then replicated on the others by implementing geometric data of each specified ellipsoid. The coordinates of each node of the particle were multiplied by the ellipsoid semilengths in the corresponding x-, y-, and z-directions. Then the nodal coordinates were updated via a rotation matrix, and finally the coordinates of each node were added to the center-point coordinates of the ellipsoid. The total number of the nodes was between 30,900 and 61,800. In the second step (contact behavior analysis), we chose "S3R" (3-node triangular, general-purpose, conventional stress/displacement shell element with reduced integration, finite membrane strains) as the element type of ellipsoidal particles, since the S3R type of element can provide accurate results in most loading situations. The reduced integration in the shell elements can form element stiffness while integrating mass matrix and distributing loadings exactly. In our three-dimension analysis, using reduced integrations not only provided relatively more accurate results but also reduced simulating times. Another important reason for choosing the

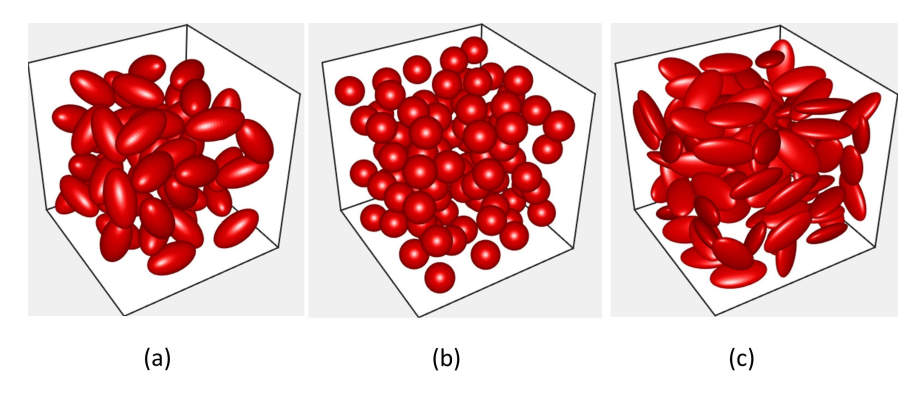


**FIG. 1:** Computer-generated models of (a) non-overlapping prolate spheroids; (b) non-overlapping of spheres; (c) non-overlapping oblate spheroids

first-order, reduced-integration elements are the best choice suitable for our solver ABAQUS/EXPLICIT® used in the contact analysis. In our third step (conduction analysis), we chose the element type "DS3" (3-node triangular, heat transfer shell element), which is available only in ABAQUS/STANDARD®. The total number of the elements was between 61,600 and 123,200.

# 2.3 Selection of Simulation Parameters

The finite element model parameters and material properties used to construct ellipsoids in the simulation process are listed in Tables 1 and 2. These were selected and combined for the purpose of achieving the numerical converging results with the fast speed based on the pre-determined solution tolerance. The simulation procedure required a large number of small time increments in the explicit analysis, in order to reduce the effect of inertia effects caused by particle compression. The selection of simulation time lengths plays an essential role in our study, as the elastic deformation of the top set of particles in the system would become so significant that they cannot transfer the loads to the bottom set if the domain walls move fairly fast. The results also would not be acceptable if the domain walls move in an absolutely slow fashion, which results in the absence of local stresses developing when the stress waves propagate over the entire system. The value of simulation time 0.4 based on the domain wall displacement 0.2 was chosen through a series of testing in our parameter study, which ensured our simulation results were independent of the compression speed of domain walls.

# 2.4 Finite Element Simulation

The two basic solvers implicit in ABAQUS/STANDARD® and explicit in ABAQUS/EXPLICIT® are commonly used in solving nonlinear mechanical problems. Although certain static or quasi-static problems that can be simulated well with either program, ABAQUS/STANDARD® may have difficulty converging in dealing with problems containing contact or material complexities, which would require excessive iterations. A large set of linear equations need to be solved in each iteration, and the iterations are repeated in each increment until the results are converged. Whereas ABAQUS/EXPLICIT® obtains the solution without iterating by explicitly advancing the kinematic state from the previous increment, even though a large number of time increments might be investigated in a certain analysis. Also, the time increment size is independent of the number of contact points and the complexity of the contact conditions in the explicit procedure. The three-dimensional models with complex contact interactions among several independent bodies always have a huge number of contacting points and the changing contact conditions simulated in our analysis would result in extremely small time increments or convergence difficulties. Thus, we, in this step, simulated the contact behavior between the deformable ellipsoidal particles via explicit finite element analysis in ABAQUS/EXPLICIT®.

The same elastic material properties were set to all the elements. Young's Modulus was set to a relatively small value to ensure the particles were soft and deformable during compression. Poisson's ratio was set to avoid surface area changes during particle compression. The parameters used in the explicit finite element analysis during particle

**TABLE 1:** Normalized parameters for contact mechanics analysis of particle compression

Simulation	Wall	Inter-particle	Particle-container	Elastic	Poisson's	Density	Shell
time	Displa-	Friction	Friction	Modulus	Ratio		Thickness/
	cement	Coefficient	Coefficient				Radius Ratio
0.4	0.2	0–1	0–1	10	0.495	$1 \times 10^{-5}$	0.15

**TABLE 2:** Normalized parameters for conduction analysis

Elastic Modulus		Conductivity	-		Gap Conductance	Gap Distance
$1 \times 10^{1}$	$1 \times 10^{-5}$	1	$1 \times 10^{-4}$	0	$1 \times 10^{6}$	$1 \times 10^{-3}$

compression are listed in Table 1. The volume fraction of particles was obtained by the sum of total particle volumes divided by the volume of the system cell corresponding at the specific position of the domain wall. During the simulation, each of the six domain walls was compressed uniformly along the x-, y-, and z-directions; the two horizontal faces, the top and the bottom faces, can only move vertically, and the four vertical side faces can only move in the horizontal direction, while all of the rest of the degrees of freedom were fixed. The system domain was compressed by the six domain walls at a constant speed, leading the system of the domain as a cubical cell during the compression simulation (Fig. 2). The surface interaction (i.e., inter-particle friction coefficient), and particle-container friction coefficient, were assigned to the contact pairs. The "all element based" option was adopted between these contact pairs for an all-inclusive element-based surface. Firstly, we investigated the contact pairs with frictionless contacting interactions in order to reduce the number of variables and simulation complexity. In the following parametrical study, we implemented the friction interactions as well as keeping some of the variables constant. The penalty friction formula was used to study the tangential behavior of contacting surfaces.

Another issue is the inhomogeneity of the system during the particle compression procedure, in which the local density of the particles near the boundary faces is not equal to the particles inside the domain. This is because the density of the outside particles starts to increase at the beginning while the density of interior remains unchanged when compressing the particles that are initially stable. This issue was resolved by assigning each particle with random initial velocities to allow them to move randomly. The analysis was performed by a set of script codes, which contained the mesh information of particles, the material properties assigned, the surface contacting interactions between particle—particle or particle—wall, the defined appropriate boundary conditions, and the prescribed loading.

# 2.5 Steady-State Conduction Analysis

In the heat transfer analysis, we considered the steady-state conduction, which was enforced by a constant temperature gradient. According to the law of heat conduction (Fourier's law), it is known that the heat conduction rate can be determined via

$$\overrightarrow{q} = -k\nabla T \tag{1}$$

where  $\vec{q}$  is the time rate of heat flux, W·m<sup>-2</sup>; k is the thermal conductivity of the material, W·m<sup>-1</sup>·K<sup>-1</sup>.  $\nabla T$  is the temperature gradient through the surface layer, K·m<sup>-1</sup>. Through the integral form as follows, we can look into the amount of thermal energy flowing through the material body:

$$\frac{\partial Q}{\partial t} = -k \iint_{S} \nabla T \cdot dS \tag{2}$$

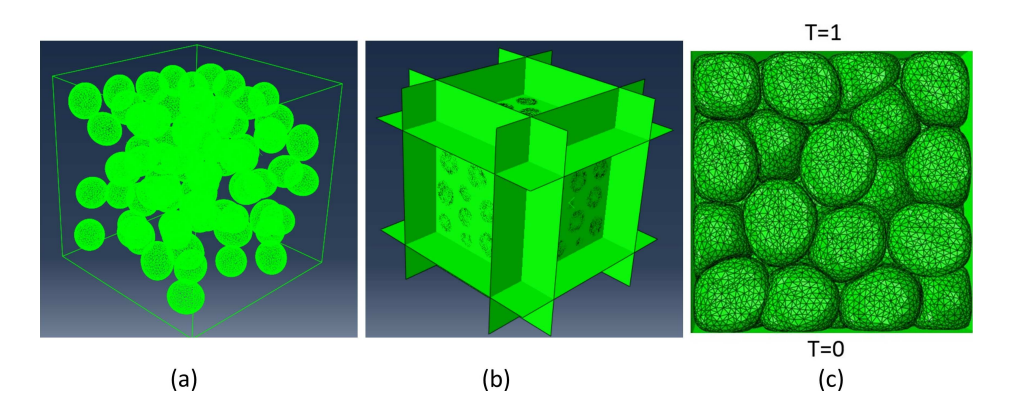


FIG. 2: Compression of the particulate system using rigid walls

where  $\partial Q/\partial t$  is the amount of heat transferred per unit time, and dS is an oriented surface area element. To perform the analysis numerically, an implicit finite element solving procedure in ABAQUS/STANDARD® is implemented, since the contact resistance (or "gap conductance") and transient analysis simulated here would lead to a more expensive way of finding solutions and a requirement for extremely small time step when using an explicit finite element procedure instead. However, before the heat conduction analysis was performed, the simulation results of the nodal displacement were exported to an ABAQUS® report file at the requested time interval (30 intervals were used actually), each of which was related to a specific value of the varying volume fractions of inclusions, or a distinct situation of the compressing cubical domain walls. The displacement results were then used to update the nodal positions of the deformed tetrahedron finite element mesh at each interval. More specifically, the appropriate boundary conditions were established in such a way that a unit temperature was defined on the top surface of the model, whereas a zero temperature was set on the bottom of the model. The reactive heat flux happened under the temperature difference, and the steady-state heat conduction was computed by solving Laplace's equation. The temperature was the single remaining degree of freedom whereas other kinetic degrees of freedom were dismissed. The pre-determined conditions implemented to classify the node for the top set or for the bottom set, which was used to assign temperature gradient, were achieved by the comparisons between z-direction coordinates of each node. The frequently used parameters in this conduction analysis are listed in Table 2. We set the coefficient of thermal expansion to zero since the effect of thermal expansion is insignificant in determining the thermal conductivity of packed powder (e.g., ceramic compounds for friction material applications). It can be demonstrated that the sum of the nodal reactive flux is equal to the effective conductivity of the whole particulate system. The reciprocal of conductance is resistance, R, given by

$$R = \frac{1}{k} = -\frac{T}{q} \tag{3}$$

The thermal contact resistance would drive the temperature to drop appreciably across the contacting interface. In general, it lowers the effective conductance as determined by either the contact stress or the normal distance between two approaching surfaces. In reality, the thermal contact resistance is a continuous function of the gap distance. For simplicity, this relationship can be approximated by a binary function in which the gap conductance is set to zero when the distance is greater than a prescribed threshold, and a nonzero constant when the distance falls below the threshold. We apply this strategy in the current study by setting the distance threshold to 0.001 to incorporate the effect of asperity contact of rough surfaces and radiation between two approach surfaces.

## 3. RESULTS

To limit the number of variables in the simulations, an infinite gap conductance or zero contact resistance is assumed in the following discussions (except Section 3.9 where the effect of gap conductance is investigated).

# 3.1 Finite Element Convergence Study

The total number of finite elements on each particle is of importance in our study since it affects both simulation accuracy and efficiency: the appropriate number of finite elements must be simulated in order to accurately describe the feature of particle interfaces, however, the computational time will increase according to a power law function of the element number. Thus, we conducted a convergence study at the beginning to investigate the sensitivity of the solution with respect to the mesh density, so that we can obtain the balance between computational accuracy and efficiency. The outcomes show that 618 nodes and 1232 elements on each particle could ensure the numerical efficiency as well as accuracy in our cases.

#### 3.2 Effect of Volume Fraction on Conductivity of Spheres

The effective conductivity was determined as a function of the volume fraction of spherical particles. Figure 3 shows a relation of the simulated effective conductivity for three different cases: (1) 120 spheres of radius 0.07; (2) 250 spheres of radius 0.055; and (3) 300 spheres of radius 0.0516. In this study, we define a dimensionless conductivity,

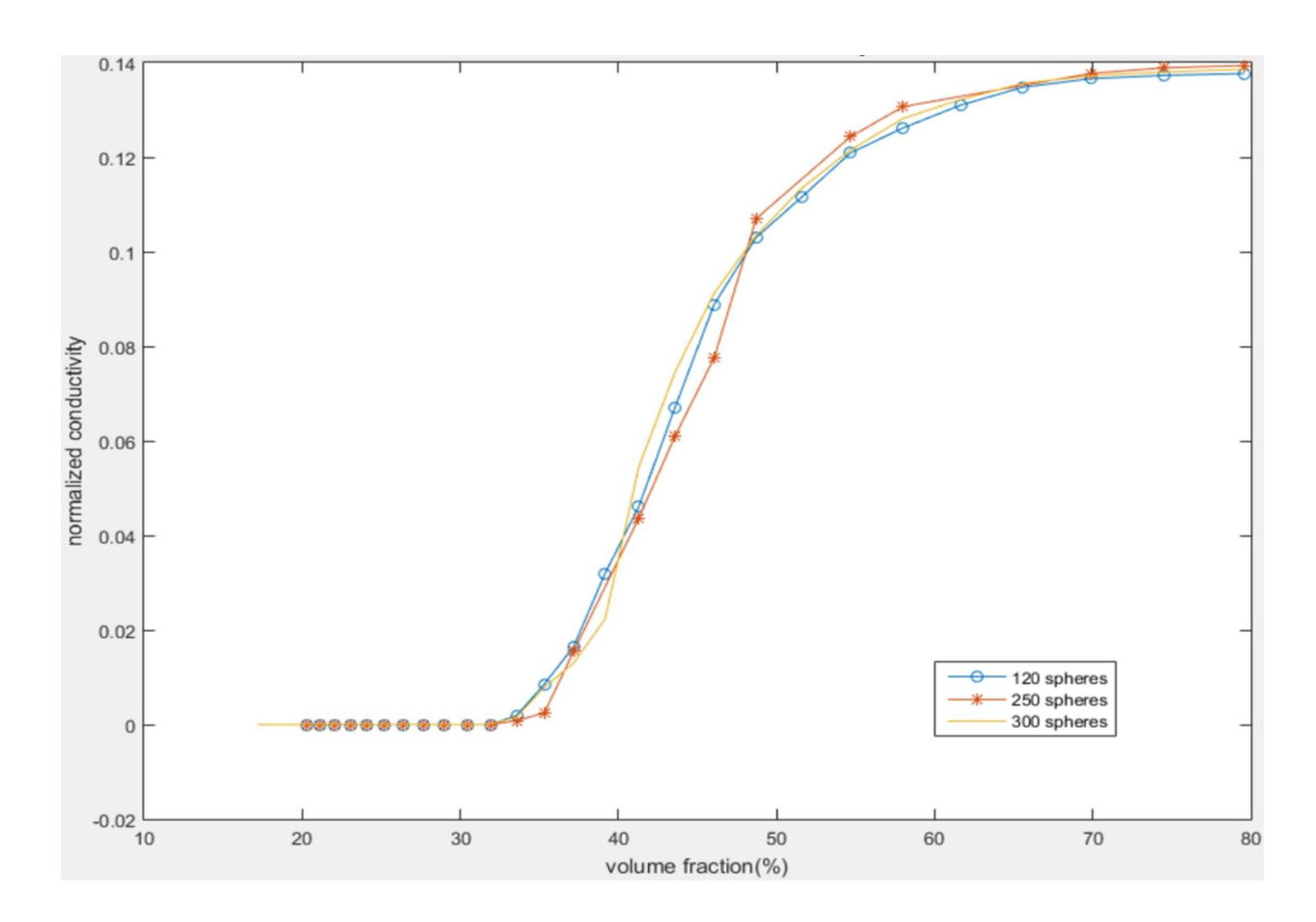


FIG. 3: Effect of particle volume fraction on conductivity

shown in Fig. 3 for example, in which it is normalized by the parameters describing the conductivity of particulate material as follows:

$$K = \frac{k_{sys}}{k_{particle}} \tag{4}$$

where  $k_{sys}$  describes the conductivity of the entire system, and  $k_{particle}$  represents the conductivity of particulate material. It can be seen that the contact model in all three cases starts to have non-zero conductivity when the volume fraction is above a certain threshold, which is located between 32% and 35% in terms of volume fraction. Below this threshold, zero conductivity was obtained since there is no conductive path formed along with the temperature distribution. Reaching this stage of the compression process, the system is considered to be "jammed" and the particles are starting to be in full contact with each other. It is clear that the volume fraction thresholds for the formation of conductive paths in all three cases are nearly the same. Above the threshold, the effective conductivity is almost a nonlinear function of the volume fraction. For example, the effective conductivity increases by 367% at 80% volume fraction compared to 40% volume fraction. At the range of 35%–60% volume fraction, the simulated results oscillate as the volume fraction increases. It is related to the fact that the contact pairs do not touch each other tightly so that there still exist some void spaces for them to adjust their locations, although they have already begun to contact with each other at this volume fraction. The irregular alteration of contact regions leads to the fluctuation of conductivity since the contact area is the only factor determining the conductivity under the infinite gap conductance assumption.

As the volume fraction increases to 65%, it is seen that the simulated results do not have much difference for all three cases. This is because the particles were in contact against each other tightly, in which the void space was rare and the variations in particle spatial locations were limited, leading to a constant value of effective conductivity. It should be pointed out that the particles are assumed to be deformable in the current study, therefore the achievable volume fraction can be as high as 100%, whereas the packing limit for random hard spheres is known to be around 64% (Torquato et al., 2000).

# 3.3 Comparison between Spheres and Ellipsoids

The intent here is to make a comparison between spherical and ellipsoidal inclusions. The averaged results with error bars are presented in Fig. 4. Two distinct cases are implemented here: (1) 120 spheres of radius 0.07; (2) 120 ellipsoids of semi-axis lengths 0.147, 0.049, 0.049 in x-, y-, z-directions, respectively. The estimated volume fraction thresholds for the formation of conductive paths for the different shapes of inclusions are very close, approximately 31% in terms of volume fraction. However, this value is much greater than the theoretical prediction reported in the literature (20%–23%) due to the scaling effect induced by a relatively small number of inclusions in the simulations. The geometric characteristics of the particles do not play an essential role, although the variations in conductivity are discernable. However, the difference between the two types of inclusions is appreciable when the volume fraction

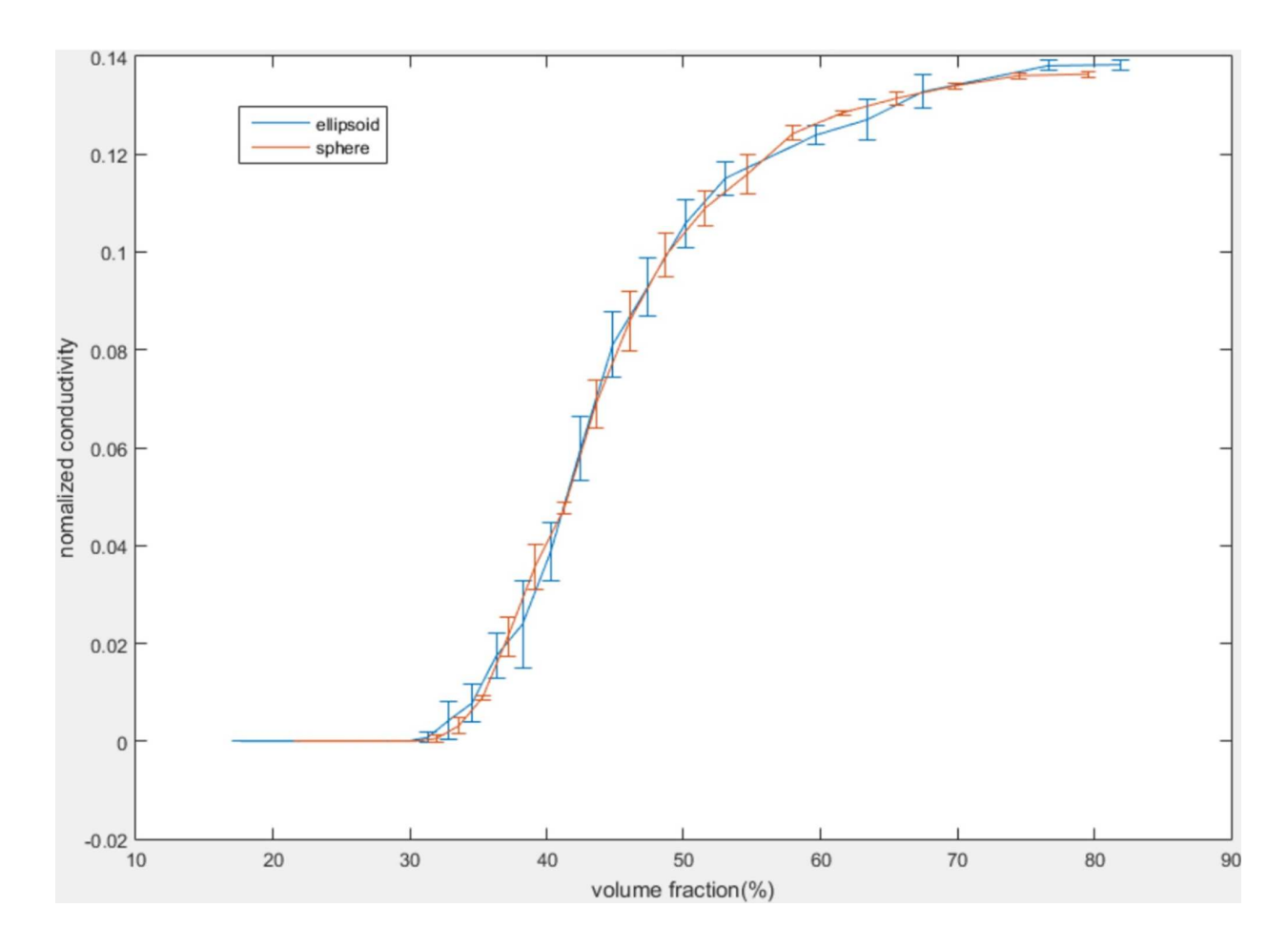


FIG. 4: Effect of particle shape on conductivity

reaches 75%. This can be explained as the distinct geometry characteristic of two different inclusions that lead to the difference in contacting regions under the compression process. A polynomial function that describes the relation between the normalized effect conductivity, K and volume fraction,  $\lambda$  for the ellipsoidal system was obtained via the least square regression method, as follows:

$$K = 5.1702 - 1.1617\lambda + 1.089\lambda^2 - 0.0056\lambda^3 + 0.0002\lambda^4$$
(5)

The corresponding function for the spherical system is

$$K = 0.983 - 0.3765\lambda + 0.0467\lambda^2 - 0.0028\lambda^3 + 0.0001\lambda^4$$
(6)

Figure 5 demonstrates how the conductive paths change under different volume fractions of a system consisting of ellipsoidal inclusions with semi-axis lengths 0.147, 0.049, 0.049, respectively. When the volume fraction is 30.5% [Fig. 5(a)], it can be seen that no conductive path is formed and the effective conductivity is zero. In addition, most of the particles are isolated from each other and rare deformation is detected. A unit temperature is uniformly distributed for those particles associated with the top domain wall, while a zero temperature is assigned to those particles connected to the bottom domain wall. As the walls progressively compress the particles to the level of jamming fraction, at least one conductive path is formed. The particles stay close to each other and most have contact regions with the adjacent pairs.

Figure 5(b) shows the deformable particles when the system volume fraction increases to 48.2% during the compression. The contact regions can be clearly seen among the deformed particles and more than one conductive path is formed. Most of the particles are interconnected with each other, and the temperature gradients for each of the conductive paths that vertically cross the system are about the same. When the volume fraction further increases to 93.6% as presented in Fig. 5(c), the elastic deformation becomes so severe that the particles can no longer retain their original shapes. The temperature gradient and heat flux along the vertically conductive paths are approximately uniformly arranged from the top side to the bottom.

# 3.4 Effect of Material Stiffness on Conductivity

We performed simulations by altering the value of dimensionless Young's Modulus while fixing Poisson's ratio to 0.495 (close to that of an incompressible material). Three identical systems of particles were maintained, and Young's Modulus was the only variable: (1) 120 spheres of radius 0.07 with dimensionless Young's Modulus 10; (2) 120 spheres of radius 0.07 with Young's Modulus 1; (3) 120 sphere of radius 0.07 with Young's Modulus 0.1. All three

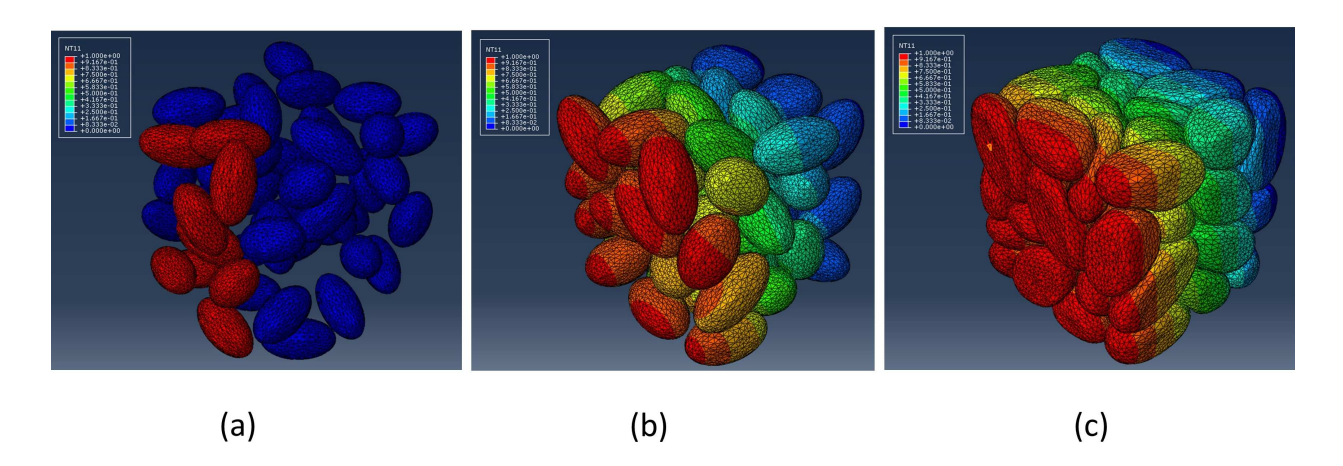


FIG. 5: Temperature field in the contact model with the following volume fractions: (a) 30.5%; (b) 48.2%; (c) 93.06%

cases show a relatively good agreement with each other, especially when the volume fraction is higher than 50%. The variation in the conductivity is greater for the stiffer material compared to the softer ones. The reactive force between contacting particles, which is responsible for the particle velocities, was supplied by the intermittent, dynamic collisions among particle–particle or particle–wall. The reactive force among particles might be larger for those of stiffer interfaces compared to the softer ones, implying that there were more frequent changes of contact regions that occurred in the stiffer ones. Thus, the results of softer particles are relatively smooth, whereas those of stiffer particles have large variations. It is observed that the material system containing soft particles can reduce the threshold for the formation of conductive paths. For example, the particulate system with normalized Young's Modulus of 1 or 0.1 has a reduction of 5% in volume fraction at this threshold in comparison with the system of Young's Modulus of 10. This might be explained by the presence of larger reactive forces between stiffer particles, causing a propulsion to provide dynamic momentum, and to facilitate the particle adjustment.

# 3.5 Effect of Prolate Ellipsoid Aspect Ratio on Conductivity

The ellipsoid aspect ratio, ε, defined as the ratio of the major semi-axis length to the minor semi-axis length, is a significant parameter that was related to describing the microstructure of a particulate material system. The geometry used in this study is assumed to be a prolate spheroid, in which the lengths of the two minor axes are equal to each other. Three distinct cases with aspect ratio of 1, 3, and 6 are investigated here, respectively, with the following parameters: (1) 120 spheres of radius 0.07; (2) 110 prolate spheroids of semi-axis lengths 0.15, 0.05, 0.05; and (3) 107 prolate spheroids of semi-axis lengths 0.24, 0.04, 0.04. These numbers of particles and semi-axis lengths were chosen to maintain the same volume fraction for all three cases. The results are shown in Fig. 6, in which the effective conductivity is a function of the aspect ratio.

It is found that the effective conductivity decreases with the ellipsoid aspect ratio at the same volume fraction. The results start to deviate from each other when the volume fraction exceeds 30%. The difference increases with the volume fraction and it is expected to have a significant discrepancy at a sufficiently high volume fraction. For example, the effective conductivity with an aspect ratio of 1 is 3.8% higher than that with an aspect ratio of 3, and 8% higher than that with an aspect ratio of 6, all at the volume fraction of 80%. Although the result is not conclusive here, it is suspected that a larger aspect ratio may impede particle adjustment, thus reducing the total contact area in comparison with spheres, leading to a lower conductivity.

# 3.6 Effect of Tri-Axial, Oblate, and Prolate Particle Shapes on Conductivity

Three types of ellipsoidal inclusions, namely tri-axial ellipsoids, oblate spheroids, and prolate spheroids, were investigated here to determine the effects of particle shapes on the effective conductivity. The following parameters were used in the simulations: (1) 83 tri-axial ellipsoids with semi-axis lengths of 0.16, 0.08, 0.04; (2) 71 oblate ellipsoids with semi-axis lengths of 0.1, 0.1, 0.06; (3) 98 prolate ellipsoids with semi-axis lengths of 0.06, 0.06, 0.12. The results are reported in Fig. 7.

It can be seen that the conductivities of the three distinct systems are very close to each other at lower volume fractions. However, they start to deviate as the volume fraction increases to around 50%. The difference becomes even larger when the volume fraction further increases. In addition, the conductivity of the prolate spheroidal system is higher than that of the oblate and tri-axial ellipsoidal systems. For example, the effective conductivity of the prolate system is 8.7% higher than that of the oblate one and 36.3% higher than that of the tri-axial system, at the volume fraction of 82%. The distinct particle morphologies in these three cases cause the difference in the contact areas thus affects the overall conductivity, especially when the particles are tightly packed.

# 3.7 Effect of Inter-Particle Friction on Conductivity

The above discussions were based on the assumption of frictionless contact, in which the alteration in the contact area was solely induced by the normal stresses due to compression. In reality, friction can play an important role and it is necessary to incorporate rough surfaces in the computational model. In particular, the existence of shear stresses

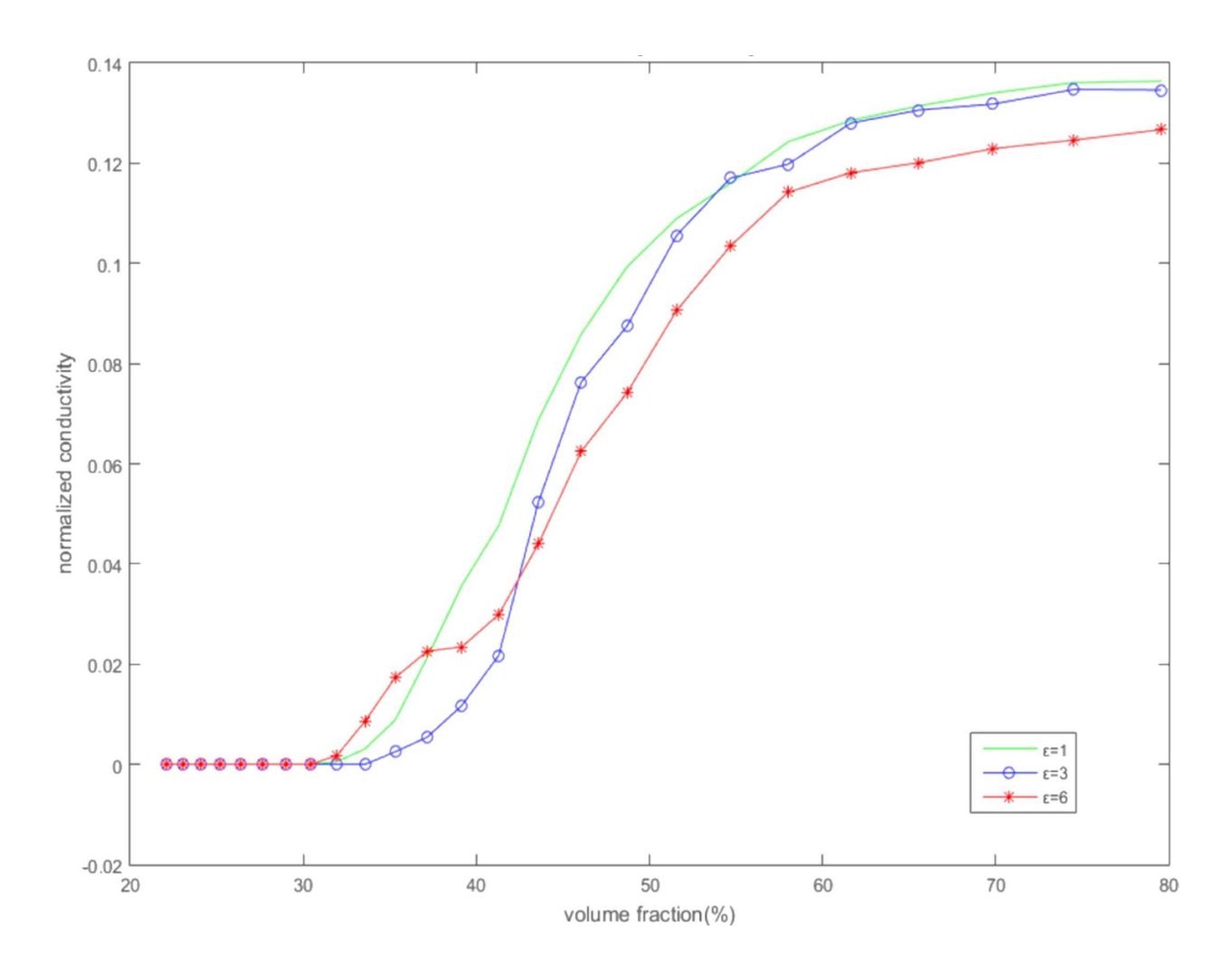


**FIG. 6:** Effect of particle aspect ratio,  $\varepsilon$  on conductivity

due to Coulomb friction leads to the shear deformation of materials in the directions parallel to the contact surfaces, thus alters the contact area. The overall thermal conductance is therefore determined not only by the applied pressure and volume fraction, but also by the coefficients of friction as well. In the current section, our prior work has been extended to involve inter-particle or particle-container frictions. A quantitative relationship was established between the conductivity and volume fraction in the following five cases: (1) 120 spheres of radius, r = 0.07 and inter-particle coefficient of friction,  $\mu 1 = 0$ ; (2) 120 spheres of r = 0.07 and  $\mu 1 = 0.15$ ; (3) 120 spheres of r = 0.07 and  $\mu 1 = 0.3$ ; (4) 120 spheres of r = 0.07 and  $\mu 1 = 0.5$ ; (5) 120 spheres of r = 0.07 and  $\mu 1 = 0.9$ . No further contact behavior was monitored for  $\mu 1 > 1$  since the particles were believed to be "sticky" enough when  $\mu 1$  is around 1. In Fig. 8, it is seen that a sudden increase in the conductivity occurs when the volume fraction is approaching a certain threshold. The values of the threshold differ in these five cases. In general, the presence of inter-particle friction lowers the volume fraction threshold at which the conductive path is formed and a sudden increase in the conductivity is obtained, due to the fact that tractions could interfere the location adjustment of particles. For example, a friction coefficient of 0.15 reduces this threshold from 34% to 32%, in terms of volume fraction. A friction coefficient of 0.3 further reduces the threshold to 31%, and a coefficient of 0.5 leads to a threshold of 30%. The maximum reduction of 5% (from 34% to 29%) occurs when  $\mu$  is set to 0.9, which is believed to be higher enough to make the particles "sticky". Above

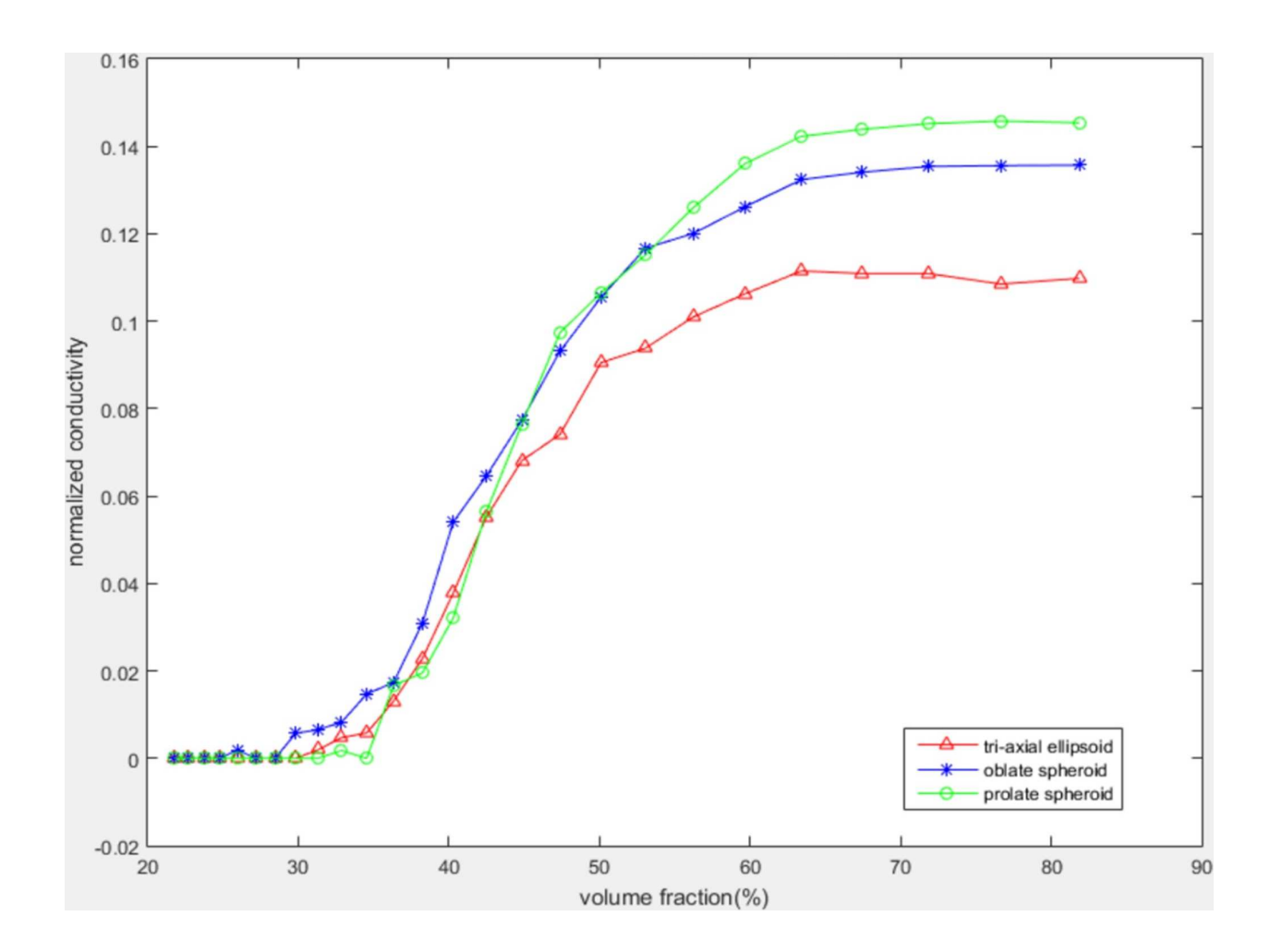


FIG. 7: Effect of geometric shape of inclusions on conductivity

this threshold, the effective conductivity increases as a nonlinear function of volume fraction. Since the frictionless contact does not impede particle adjustment, rapid changes of contact regions and thus a large standard deviation in the conductivity is observed. The system undergoes energy dissipation in the presence of friction, leading to a reduction in the variations in the results. It is found that the conductivity of the frictionless contact model is lower than that of the friction contact model when the volume fraction is between 40% and 55%. When the compression continues and the volume fraction is exceeding 60%, all five curves flatten due to suppression in the variations of the contact areas, although a slight difference between them is discernable. It can also be seen that there is a crossover in the result showing that the conductivity decreases with the friction coefficient when the volume fraction exceeds 60%.

# 3.8 Effect of Particle-Container Friction on Conductivity

The effect of the Coulomb friction between the particles and the container walls was also investigated. Figure 9 shows the simulated effective conductivity as a function of the volume fraction in the following five cases: (1) 120 spheres of radius, r = 0.07 and the coefficient of particle-container friction,  $\mu 2 = 0$ ; (2) 120 spheres of r = 0.07 and  $\mu 2 = 0.15$ ; (3) 120 spheres of r = 0.07 and  $\mu 2 = 0.3$ ; (4) 120 spheres of r = 0.07 and  $\mu 2 = 0.5$ ; (5) 120 spheres of r = 0.07 and  $\mu 2 = 0.9$ .

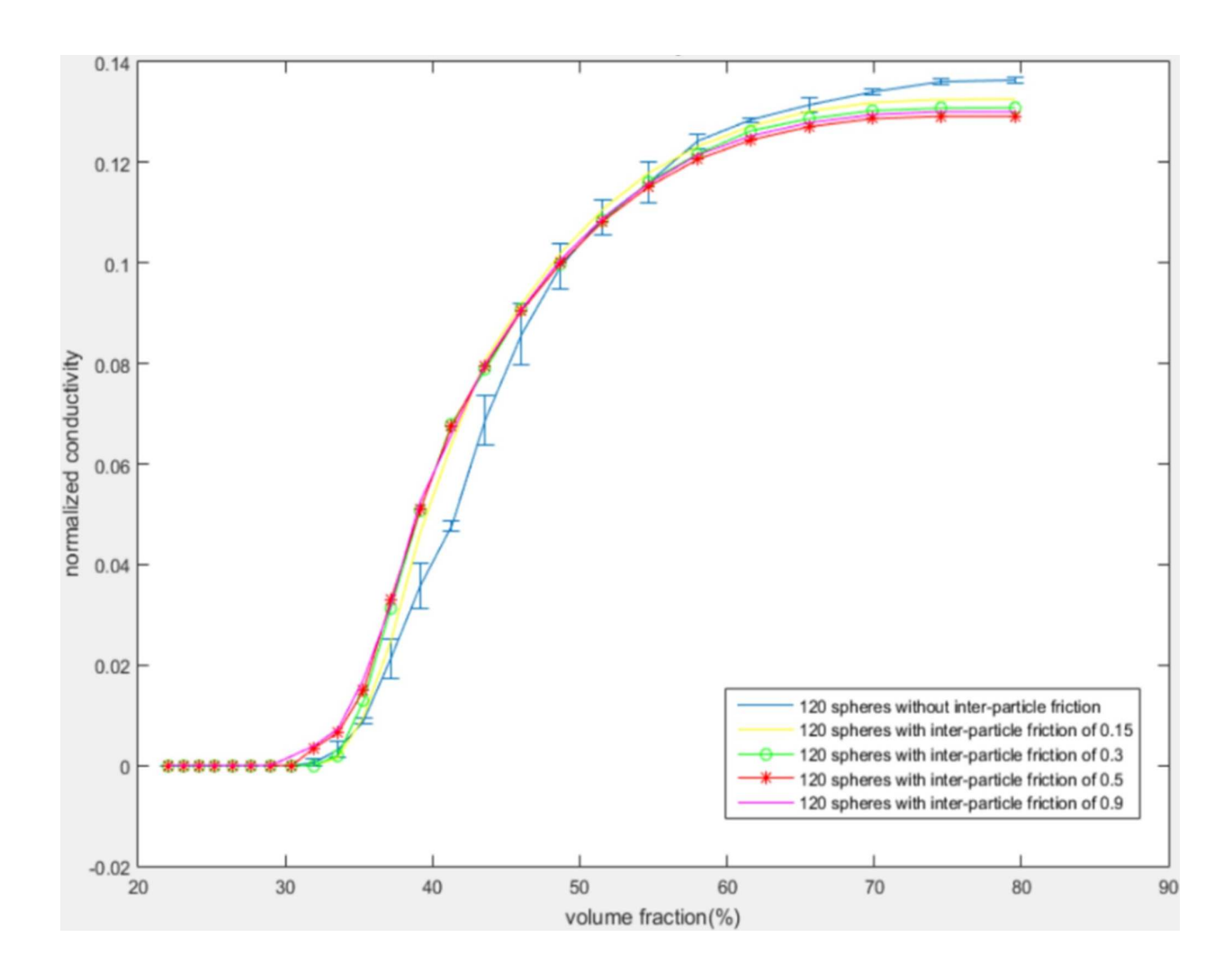


FIG. 8: Effect of inter-particle friction coefficient, μ1 on effective conductivity (with error bars)

The results show a similar pattern compared with the inter-particle friction cases. It is found that the presence of particle-container friction lowers the volume fraction threshold for the formation of conductive paths due to the impediment of particle location adjustment, although the effects are not as significant as that in the inter-particle friction cases. Above this threshold, the conductivity of the frictionless contact model is lower than that of the frictional contact model, due to the increased contact areas in the latter case.

# 3.9 Effect of Gap Conductance on Conductivity

The aforementioned results were based on the assumption of infinite gap conductance or zero contact resistance, in which the alteration of the contact area is the only factor that affects the overall conductivity. In a more realistic material system, the contact resistance is inevitable due to the rough surfaces of particles caused by the compression or mixing processes. Further, contact resistance can also come from a perfectly smooth, but oxidized surfaces, as in the aluminum oxide layer on aluminum particles. In both cases, the contact resistance can be characterized as a gap conductance with a finite value. Here we have determined the relationship between the gap conductance and the effective conductivity. A special case involving 120 spheres of radius, r = 0.07 with the gap conductance as the

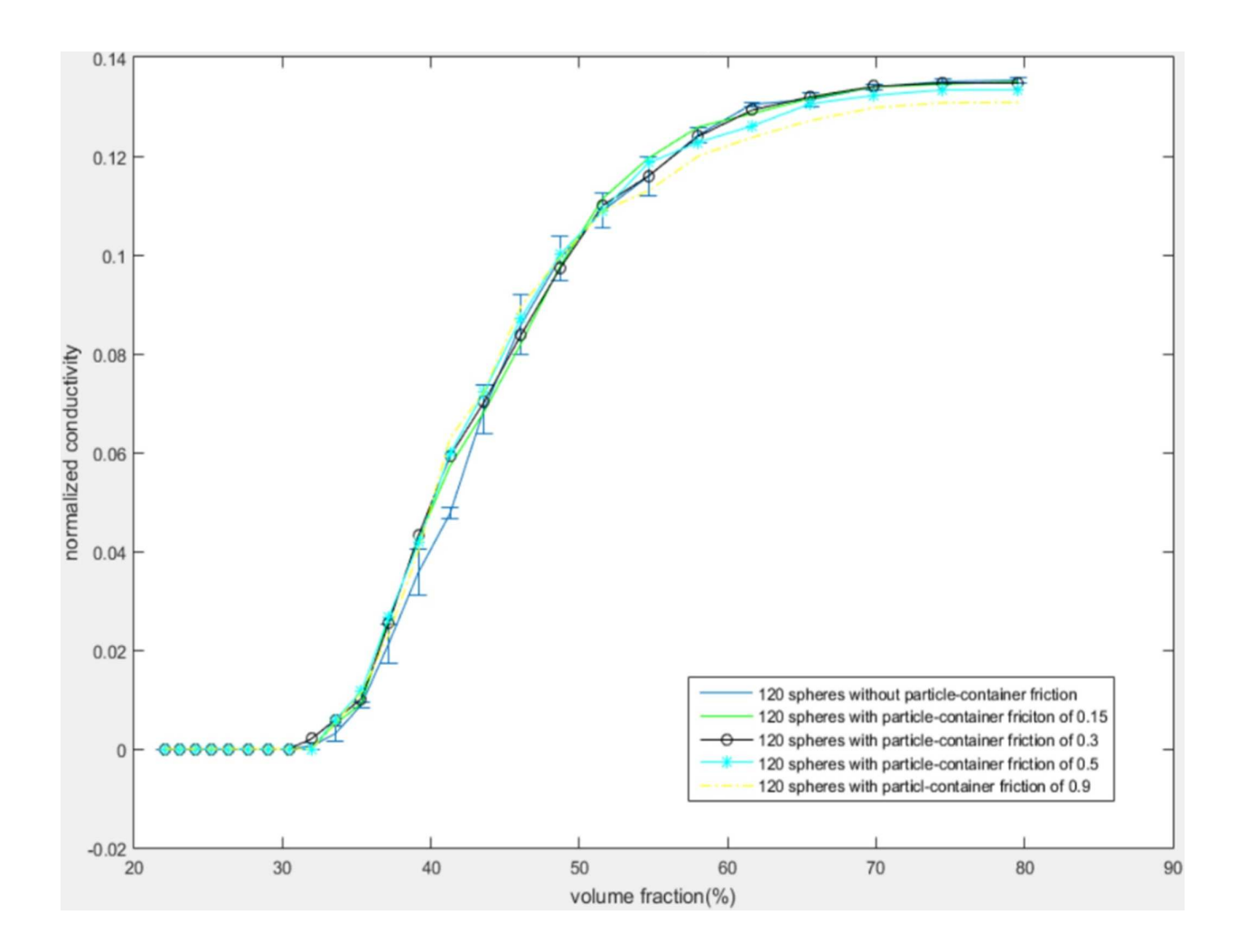


FIG. 9: Effect of container-particle friction coefficient, μ2 on effective conductivity (with error bars)

only variable that varies from 1 to  $10^6$  was studied. The thermal conductivity is shown as a function of the volume fraction under the difference gap conductance in Fig. 10. On the other hand, Fig. 11 presents the relation between the gap conductance and the thermal conductivity when the volume fraction is set to 80%. Clearly as expected, the gap conductance has lowered the effective conductivity. When the volume fraction is sufficiently high, the difference could be significant. For example, the dimensionless thermal conductivity is 0.03 at the gap conductance of 1, which decreases by 77% compared to the case assuming an infinite gap conductance. However, the thermal conductivity is independent of gap conductance when it exceeds a magnitude of  $10^3$  and the overall thermal conductivity approaches zero when the gap conductance is sufficiently small. This is because the overall thermal conductivity in a bi-material system is always dominated by the poor conductor. Finally, the nonlinearity in the curves is a collective effect caused by both the thermal conductivity of particle material and the interfacial contact resistance.

## 4. CONCLUSIONS AND FUTURE WORK

In manufacturing of particulate friction materials, the particle morphologies, the orientation angles of the grains, and the local deformation can be altered through different processes. In this study, a dynamic collision algorithm was successfully implemented to simulate the effective thermal conductivity based on the Monte Carlo method and the

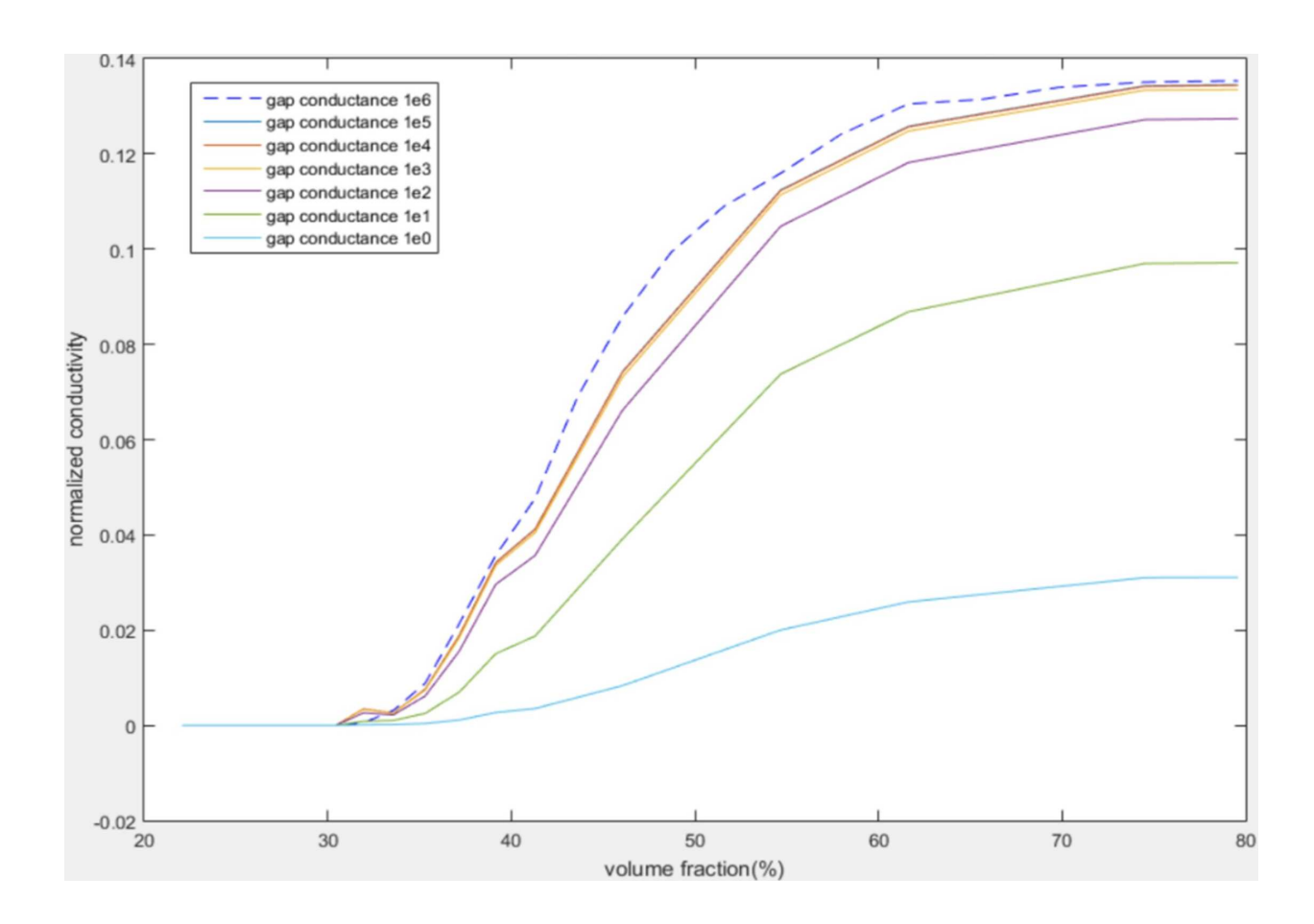


FIG. 10: Effect of gap conductance on effective conductivity

finite element scheme. The contact among deformable particles not only included the basic contact mechanics but also the interfacial Coulomb friction and contact resistance. Several conclusions have been obtained as follows:

- 1. A quantitative relationship is obtained between the volume fraction and the effective conductivity. A large variation is observed for a finite system due to the rapid change in contacting area among particles while they are experiencing location adjustment during compression.
- 2. The effects of material stiffness cannot be neglected. The simulation results show a greater variability in the conductivity for "hard" particles compared with "soft" ones.
- 3. The conductivity decreases with the aspect ratio of particles, especially at high volume fractions. The discrepancies among particles of different shapes increase with the volume fraction.
- 4. An analysis of the effect of morphological shapes (i.e., tri-axial, prolate, or oblate ellipsoids) reveals that the prolate inclusions produce the highest effective conductivity over the oblate particles or tri-axial ellipsoids at high volume fractions.
- 5. The presence of interfacial friction can change the conductivity via impeding the relative motion among particles and causing local deformation of particle surfaces.

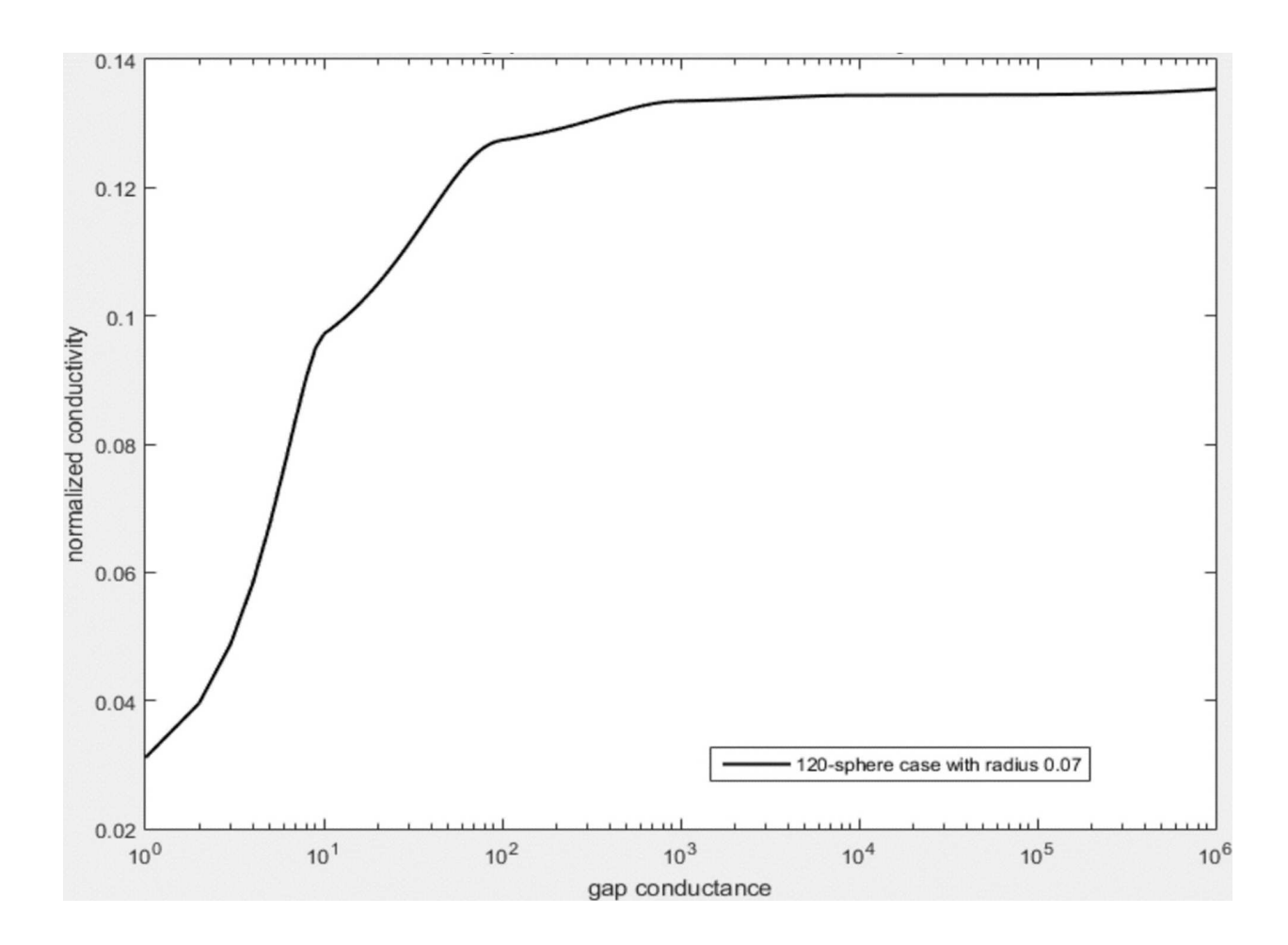


FIG. 11: Effective conductivity as a function of gap conductance at volume fraction of 80%

6. The gap conductance decreases the effective conductivity. However, the conductivity becomes independent of the gap conductance when the normalized value exceeds the order of magnitude approximately 10<sup>3</sup>.

The above findings are particularly important in predictive modeling of friction materials consisting of graphite or ceramic particles for the prevention of thermal instability. Our intention of the current study is to develop a methodology to study the effect of contact resistance on thermal conductivity. There should be a scaling or size effect that may impact the applicability of the results at a different scale, but our tentative work shows the same trend in the simulation results. Future work will involve modeling the pressure-dependent contact resistance, as well as the effect of thermal expansion at elevated temperatures in the presence of frictional heating.

#### **ACKNOWLEDGMENT**

Support for this work, partially provided by the National Science Foundation under Contract No. 1928876, is gratefully acknowledged.

# **REFERENCES**

ABAQUS USERS MANUAL, Dassault Systèmes Simulia Corp. Providence, RI, USA, 2019.

- Aranganathan, N. and Bijwe, J., Comparative Performance Evaluation of NAO Friction Materials Containing Natural Graphite and Thermo-Graphite, *Wear*, vols. **358–359**, pp. 17–22, 2016.
- Cai, W., Tu, S., and Tao, G., Thermal Conductivity of PTFE Composites with Three-Dimensional Randomly Distributed Fillers, J. Thermoplastic Comp. Mat., vol. 18, pp. 241–253, 2005.
- Chen, J., Xu, L., and Li, H., Investigation on a Direct Modeling Strategy for the Effective Elastic Moduli Prediction of Composite Material, *Mat. Sci. Eng. A*, vol. **491**, pp. 385–389, 2008.
- Cheng, X. and Sastry, A.M., On Transport in Stochastic, Heterogeneous Fibrous Domains, *Mech. Mater.*, vol. **31**, pp. 765–786, 1999.
- Fish, J. and Fan, R., Mathematical Homogenization of Nonperiodic Heterogeneous Media Subjected to Large Deformation Transient Loading, *Int. J. Numer. Methods Eng.*, vol. **76**, pp. 1044–1064, 2008.
- Garboczi, E.J. and Berryman, J.G., Elastic Moduli of a Material Containing Composite Inclusions: Effective Medium Theory and Finite Element Computations, *Mech. Mat.*, vol. **33**, pp. 455–470, 2001.
- Gubernatis, J.E. and Krumhansl, J.A., Macroscopic Engineering Properties of Polycrystalline Materials—Elastic Properties, J. Appl. Phys., vol. 46, pp. 1875–1883, 1975.
- Kansal, A.R., Torquato, S., and Stillinger, F.H., Computer Generation of Dense Polydisperse Sphere Packings, *J. Chem. Phys.*, vol. 117, pp. 8212–8218, 2002.
- Kaźmierczak-Baiata, A. and Mazur, J., Effect of Carbon Nanoparticle Reinforcement on Mechanical and Thermal Properties of Silicon Carbide Ceramics, *Ceramics Int.*, vol. **44**, pp. 10273–10280, 2018.
- King, W.E., Anderson, A.T., Ferencz, R.M., Hodge, N.E., Kamath, C., Khairallah, S.A., and Rubenchik, A.M., Laser Powder Bed Fusion Additive Manufacturing of Metals; Physics, Computational, and Materials Challenges, *Appl. Phys. Rev.*, vol. 2, no. 041304, 2015. DOI: 10.1063/1.4937809
- Li, P., Li, T., and Yan, H., Mechanical, Tribological and Heat Resistant Properties of Fluorinated Multi-Walled Carbon Nanotube/Bismaleimide/Cyanate Resin Nanocomposites, *J. Mat. Sci. Technol.*, vol. **33**, pp. 1182–1186, 2017.
- Lu, Y., A Combinatorial Approach for Automotive Friction Materials: Effects of Ingredients on Friction Performance, *Compos. Sci. Technol.*, vol. **66**, pp. 591–598, 2006.
- Maxwell, J.C., A Treatise on Electricity and Magnetism, Oxford, UK: Clarendon Press, 1873.
- Mclaughlin, R., Study of Differential Scheme for Composite-Materials, Int. J. Eng. Sci., vol. 15, pp. 237–244, 1977.
- Mondescu, R.P. and Muthukumar, M., Effective Elastic Moduli of a Composite Containing Rigid Spheres at Nondilute Concentrations: A Multiple Scattering Approach, *J. Chem. Phys.*, vol. **110**, pp. 1123–1137, 1999.
- Mussatto, A., Groarke, R., O'Neill, A., Obeidi, M.A., Delaure, Y., and Brabazon, D., Influences of Powder Morphology and Spreading Parameters on the Powder Bed Topography Uniformity in Powder Bed Fusion Metal Additive Manufacturing, *Add. Manufact.*, vol. 38, no. 101807, 2021. DOI: 10.1016/j.addma.2020.101807
- Panda, J.N., Bijwe, J., and Pandey, R.K., Role of Treatment to Graphite Particles to Increase the Thermal Conductivity in Controlling Tribo-Performance of Polymer Composites, *Wear*, vols. **360–361(C)**, pp. 87–96, 2016.
- Pike, G.E. and Seager, C.H., Percolation and Conductivity: A Computer Study, Phys. Rev. B, vol. 10, pp. 1421-1434, 1974.
- Qiu, J., Williams, J., and Yi, Y.B., Random Walk Based Stochastic Modeling of Diffusion in Spherical and Ellipsoidal Composites, Int. J. Multiscale Comput. Eng., vol. 18, pp. 493–505, 2020.
- Qiu, J. and Yi, Y.B., Random Walk Simulation Model of Diffusion in Circular and Elliptical Particulate Composites, *Int. J. Multiscale Comput. Eng.*, vol. 16, pp. 131–142, 2018.
- Qiu, J., Yi, Y.B., and Guo, X., Computational Prediction of Electrical and Thermal Conductivities of Disklike Particulate Composites, *Int. J. Comput. Mat.*, vol. 4, no. 1550013, 2015.
- Singaravelu, D.L., Rahul, R.M., Vijay, R., Manoharan, S., and Kchaou, M., Development and Performance Evaluation of Eco-Friendly Crab Shell Powder Based Brake Pads for Automotive Applications, *Int. J. Auto. Mech. Eng.*, vol. 16, pp. 6502–6523, 2019.
- Solomon, D.G. and Berhan, M.N., Characterization of Friction Material Formulations for Brake Pads, Proc. World Cong. Eng. Vol. II WCE 2007, London, UK, July 2-4, 2007.
- Song, Y.S. and Youn, J.R., Evaluation of Effective Thermal Conductivity for Carbon Nanotube /Polymer Composites Using Control Volume Finite Element Method, *Carbon*, vol. **44**, pp. 710–717, 2006.

Sriwiboon, M., Tiempan, N., and Kaewlob, K., Non-Asbestos Organic (NAO) Disc Pad Wear Behavior: Divergence of Thickness Loss and Weight Loss, *SAE Tech. Paper*, 2018-01-1866, 2018. DOI: 10.4271/2018-01-1866

- Sykes, M.F. and Essam, J.W., Some Exact Critical Percolation Probabilities for Bond and Site Problems in 2 Dimensions, *Phys. Rev. Lett.*, vol. **10**, pp. 3–4, 1963.
- Tawerghi, E. and Yi, Y.B., A Computational Study on the Effective Properties of Two-Phase Heterogeneous Media Containing Particulate Inclusions, *J. Physics D: Appl. Phys.*, vol. **42**, no. 175409, pp. 1–10, 2009.
- Torquato, S. and Rintoul, M.D., Effect of the Interface on the Properties of Composite Media, *Phys. Rev. Lett.*, vol. **75**, pp. 4067–4070, 1995.
- Torquato, S., Random Heterogeneous Materials, Springer-Verlag, Inc., New York, 2002.
- Torquato, S., Truskett, T.M., and Debenedetti, P.G., Is Random Close Packing of Spheres Well Defined? *Phys. Rev. Lett.*, vol. **84**, pp. 2064–2067, 2000.
- Volpp, J., Powder Particle Movement during Powder Bed Fusion, Proc. Manufact., vol. 36, pp. 26–32, 2019.
- Wang, C.W., Yi, Y.B., and Sastry, A.M., Particle Compression and Conductivity in Li-Ion Anodes with Graphite Additives, *J. Electrochem. Soc.*, vol. **151**, pp. A1489–A1498, 2004.
- Wei, C.Y., Srivastava, D., and Cho, K., Structural Ordering in Nanotube Polymer Composites, *Nano Lett.*, vol. 4, pp. 1949–1952, 2004.
- Wei, E.B. and Poon, Y.M., Effective Thermal Conductivity of Graded Nonlinear Composites with Heat Contact Resistance, *Phys. Lett. A*, vol. **359**, pp. 685–692, 2006.
- Ye, P., Wu, J., Mu, L., He, D., Feng, X., and Lu, X., Tribological Behaviors of Carbon Series Additions Reinforced CF/PTFE Composites at High Speed, J. Appl. Polymer Sci., vol. 133, no. 20, 2016. DOI: 10.1002/app.43236
- Yi, Y.B., The Role of Interparticle Contact in Conductive Properties of Random Particulate Materials, Acta Mat., vol. 56, pp. 2810–2818, 2008.
- Yi, Y.B., Wang, C.W., and Sastry, A.M., Compression of Packed Particulate Systems: Simulations and Experiments in Graphitic Li-Ion Anodes, *ASME J. Eng. Mat. Tech.*, vol. **128**, pp. 73–80, 2006.
- Yi, Y.B., Wang, C.W., and Sastry, A.M., Two-Dimensional versus Three-Dimensional Clustering and Percolation in Fields of Overlapping Ellipsoids, J. Electrochem. Soc., vol. 151, pp. A1292–A1300, 2004.
- Yi, Y.B. and Tawerghi, E., Geometric Percolation Thresholds of Interpenetrating Plates in Three-Dimensional Space, *Phys. Rev. E*, vol. **79**, no. 041134, 2009.
- Zhang, T. and Yi, Y.B., A Monte Carlo Simulation of Effective Electrical Conductivity in Coated Fibers, J. Appl. Phys., vol. 103, no. 014910, 2008.
- Zhao, J., Yi, Y.B., and Li, H., Effects of Frictional Material Properties on Thermoelastic Instability Deformation Modes, *J. Eng. Tribol.*, vol. **229**, pp. 1239–1246, 2015.